A TOTAL QUALITY ASSESSMENT SOLUTION FOR SYNTHETIC APERTURE RADAR NLFM WAVEFORM GENERATION AND EVALUATION IN A COMPLEX RANDOM MEDIA

Iman Heidarpour Shahrezaei, Morteza Kazerooni, Mohsen Fallah

Electrical and Electronic Engineering Department (EEED)

Malek Ashtar University of Technology (MUT), P.O.B:115/83145

Lavizan, Tehran, Iran

Emails: Heidarpour@mut.ac.ir, Kazerooni@mut.ac.ir, Mohsen_fallah@mut.ac.ir

Submitted: Dec. 15, 2016 ***Accepted: Feb. 17, 2017*** ***Published: Mar. 1, 2017***

Abstract- A Design, simulation and optimal selection of non-linear frequency modulation waveforms (NLFM) based on correlated ambiguity function (AF) quality analysis for the purpose of Synthetic Aperture Radar (SAR) is done in this article. The selected optimum CNLFM waveform in contribution with other waveforms are applied directly into a SAR image formation algorithm (IFA) and their quality metrics in comparison to other waveforms are derived and analyzed in a complex random media (CRM). The total quality performance analysis includes both the qualitative AF diagrams and the objective image quality metrics assessments. The simulation results not only verify the robustness of the proposed NLFM waveforms as a suitable alternative for LFM waveform but also introduce NLFM as a proper method of modulation for SAR in CRM.

Index terms*:* Synthetic Aperture Radar (SAR), Non-Linear Frequency Modulation (NLFM), Ambiguity Function (AF), image formation algorithm (IFA), complex random media (CRM), quality assessment techniques.

I. INTRODUCTION

Synthetic aperture radar (SAR) image formation is based on a coherent processing approach to build a 2D-image with the application in the field of remote sensing, explorations, agriculture, military, etc., in all weather and all time [1-3]. This coherent processing also known as the compression of frequency modulated pulse. This allows more energy to be transmitted and also better range resolution to be achieved. The range compressed pulse is obtained by means of correlation of received echo with the complex conjugate time-inverted replica of the transmitted pulse, also known as linear time invariant (LTI) analysis [4]. SARs are available in different application modes like spotlight SAR, stripmap SAR, squinted stripmap or spotlight SAR, interferometric SAR (InSAR) and inverse SAR (ISAR) which depends on the operation, environment, target condition and image resolution [5]. Due to its versatile applications, airborne with high speed flight characteristics can be equipped with this technique [6-9]. Linear FM signals (LFM) signals are very important in microwave imaging and SAR systems, where the signal's instantaneous frequency is a continuous linear modulation function of time to achieve a uniformly filled bandwidth [6-10]. The match filter response of LFM has a side-lobe level of -13dB, which can be improved by some methods but at costs reducing SNR and wider main-lobe, which make it improper to use in SAR image formation [11]. On the other hand, Non-linear LFM (NLFM) is another alternative which provides finer resolution, better SNR and good interference mitigation with the help of spectrum weighting [5, 12-17]. The NLFM technique has been used such as discrete and continuous signal modulation [12-13]. Continuous NLFM waveforms with the help of phase modulation were devised in a way that provides very smaller side-lobe level, as well as the ability to be designed on hardware structures in contrast to discrete signal modulation [14-17]. In [14], the NLFM is designed based on piecewise linear (PWL) functions as a method of instantaneous frequency function to generate the NLFM while no quality analysis is done for the NLFM design procedure per se. The radar ambiguity function (AF) provides an indication of the limitations and utility of different waveforms while assess the properties of the transmitted waveform regarding to its target resolution, measurement accuracy, ambiguity and responses to the backscattering [12, 15, 19]. The AF is probably the most complete quality assessment statement of the waveform's inherent performance. In [14, 16-17], the NLFM is just used in an image formation algorithm (IFA) and don't consist any further AF quality analysis diagrams and metrics on the waveform designing and implementation. In this study, NLFM waveform design

consideration based on AF quality analysis is firstly presented. Then, in comparison to [13-17] two major different NLFM waveforms are not only simulated and evaluated based on AF quality analysis, but also were directly implemented to the SAR IFA for further objective quality assessment metrics assessment in the complex random media (CRM). The total quality assessment solution based on qualitative AF diagrams extraction besides the objective quantitative IFA metric assessment based on 2D-image verification is a complete routine not only have not been used but also have been neglected [12-17]. The qualitative AF analysis of the optimal SAR continuous NLFM waveform is done via ambiguity diagram extraction [18], while the quantitative metric assessment is done via the calculation of mean value, variance, mean square errors (MSE), signal-to-noise ratio (SNR), peak SNR (PSNR), structural similarity index map (SSIM), power spectral density (PSD), normalized cross correlation (NCC) and integrated side lobe ratio (ISLR) [19-21]. Fig.1 shows a low squinted stripmap SAR with its simple LTI model in receive as one of the common types of airborne SARs with high imaging resolution.

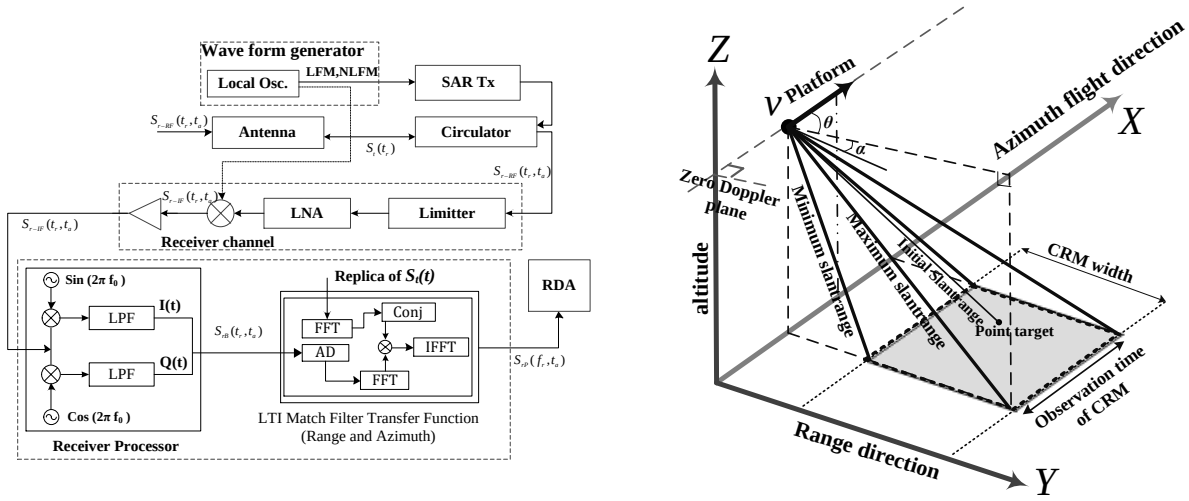

Figure 1. The low squinted high-speed SAR flight geometry and its LTI model in receive

This paper organized as follows. Firstly, both the LFM and the continuous NLFM waveforms are modeled based on AF analysis. Section.II, also introduces the proposed optimum continuous NLFM waveform selection based on AF quality analysis as well as its raw data generation. Section.III, utilizes a range-Doppler algorithm (RDA) to generate the images of the proposed optimum cosine NLFM (CNLFM), while images of other waveforms were produced indeed. Section.IV, contains complete objective quality metric assessment techniques for evaluation of CNLFM waveform application in 2D-SAR images in CRM, While images of other waveforms

are used in this analysis and compared. Section.V, presents conclusions on the NLFM simulation results while dealing with CRM and proposed topics for further researches.

II. CONTINUOUS NLFM WAVEFORM QUALITY ANALYSIS BASED ON CORRELATED AF

This section on the basis of correlated AF simulates LFM and NLFM waveforms ambiguity diagrams while including qualitative AF analysis.

a. LFM and NLFM waveform design considerations

The pulse compression method is the best technique to increase range resolution meanwhile SNR remains suitable in the receive process. The general form of LFM waveform is:

$$S_t(t) = \text{A}.rect\left(\frac{t}{T}\right)\cos(2\pi f_0 t + \pi K_r t^2) \quad (1)$$

Where, T represents the radar pulse width, f_0 is the carrier frequency, K_r is the chirp rate or the slope of the frequency alteration and $A.rect\left(\frac{t}{T}\right)$ is the signal amplitude modulation term, while the quadratic phase modulation presented as (2):

$$\varphi(t) = 2\pi f_0 t + \pi K_r t^2 \quad (2)$$

The LFM waveform complex envelope with both amplitude and phase modulation can be shown as Fig. 2 in terms of equation (3):

$$s(t) = A\ rect\left(\frac{t}{T}\right)e^{j\pi K_r t^2} \quad (3)$$

If the LFM waveform is designed in a way that its frequency alters asymmetrically within the bandwidth, the quadratic phase modulation is changed as Eq. (4), which is called continuous NLFM:

$$\varphi(t) = 2\pi f_0 t + K_r t^2 + \omega_n(t) \quad (4)$$

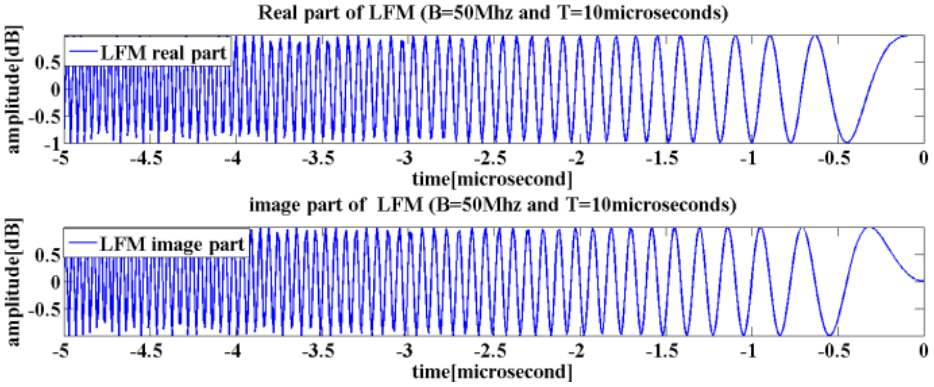

Figure 2. Typical LFM waveform complex envelope

Where $\omega_n(t)$ defines the non-linearity behavior of quadratic phase modulation of the waveform in shape of sine, cosine, tangent and etc. Fig.3 shows how the frequency alters within the time while the sine, the cosine and conventional linear functions are used.

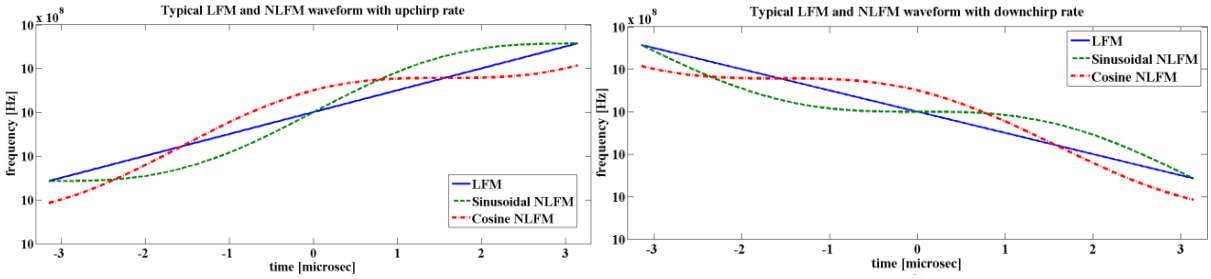

Figure 3. Frequency alteration of LFM and NLFM waveforms (a) up chirp (b) down chirp

It should be noted that both the continuous sine NLFM (SNLFM) and the continuous cosine NLFM (CNLFM) have the same complex envelope similar to the LFM, but with different amplitude at the same times because of non-linearity characteristics of the frequency alteration. These non-linear frequency alterations in continuous NLFM waveform, will lead to spectral weighting and cause the waveform does not have the SNR loss in contrast to LFM [12]. Also, NLFM has better detection rate characteristics and is more accurate in range determination than LFM which makes it suitable for SAR application [22]. With the recent progress in the field of high speed digital-to-analogue (A/D) and signal processing, generating high performance and precise NLFM waveform in SAR application is recommended more than previous. The aim of the part.b is to synthesize qualitatively the LFM, continuous SNLFM and continuous CNLFM waveforms based on correlated AF diagrams.

b. LFM and continuous NLFM qualitative analysis based on AF

Radar waveform AF is the output response of a matched radar receiver to a single point scatterer at all possible combination of ranges and velocities. The AF is also used to assess the properties of the transmitted waveform with regards to its radar resolution and target terrain backscattered responses. The AF of the SAR waveform can be defined in terms of cross-correlation of Doppler-shifted version of the waveform in the delay time and Doppler frequency plane (τ, f_d). The AF of transmitted waveform, $S_t(t)$, is defined as:

$$|\chi(\tau; f_d)|^2 = \left|\int_{-\infty}^{+\infty} S_t(t) S_t^*(t-\tau) e^{j2\pi f_d t} dt\right|^2 \quad (5)$$

Where, τ is the delay time and f_d is the Doppler frequency shift. According to Eq. (1) and Eq. (5), the AF of the LFM pulse can finally be written as Eq. (6):

$$|\chi(\tau; f_d)| = \left|\left(1 - \frac{\tau}{T}\right) sinc[\pi T(1 - \tau/T)(f_d + k_r\tau)]\right| \qquad |\tau| \le T \tag{6}$$

This relation contains both the LFM ambiguity diagram and the LFM ambiguity contour levels which are shown in Fig. 4. It also depicts rotated identical ambiguity contour level which is due to the delay time and the chirp rate slope of the waveform as shown in Fig.3. Due to the similar inherent specifications of the continuous NLFM in comparison to the LFM, obtaining similar ambiguity diagram is expected. Whatsoever, different frequency chirp rate of the waveforms will lead to different ambiguity contour levels with different spectral weighing. Hence, presenting the AF diagrams of continuous NLFM waveforms in comparison to its LFM counterpart is a proper method for quality analysis based on AF diagrams extraction.

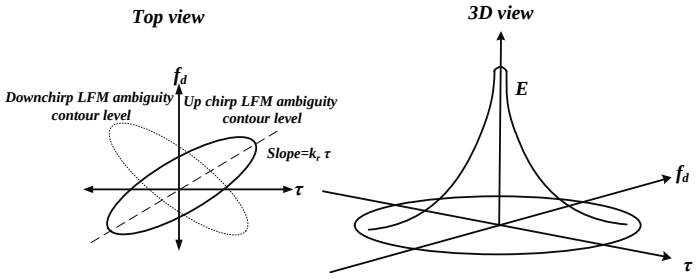

Figure.4. 3D-view of ambiguity diagram and its pertinent ambiguity contour level

According to Eq. (1), Eq. (5) and Eq. (6) the LFM waveform AF diagrams are derived as Fig. 5.

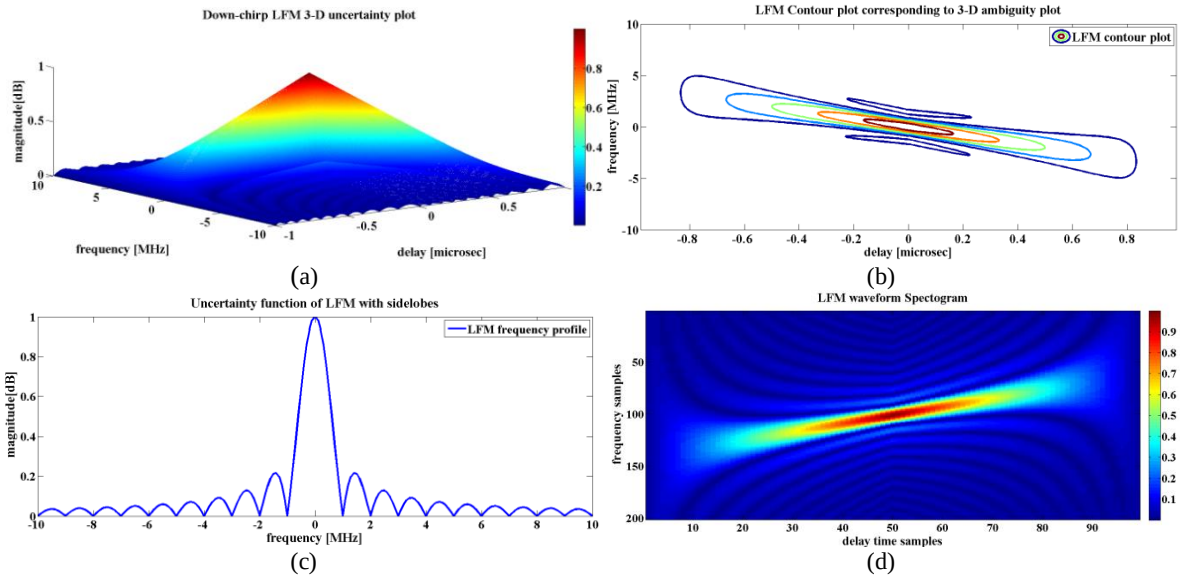

Fig.5. Typical LFM waveform AF simulation results (a) ambiguity diagram (b) ambiguity contour levels (c) AF frequency profile (d) AF spectrogram

The same qualitative AF analysis for both of the continuous SNLFM and the continuous CNLFM are also done, which are presented in Fig.6. The results show that the main-lobe of frequency

profile for both of the SNLFM and the CNLFM is twice bigger than their similar LFM waveform. On the other hand, the CNLFM frequency profile has distinctive lower side-lobe level ratio in comparison to the SNLFM which makes it suitable for SAR image formation application. The AF contour levels of CNLFM not only differs from the SNLFM but also is slightly more compact than LFM waveform which leads in less spectral expansion of adjacent pixels and helps to improve the quality on the basis of spectral weighing.

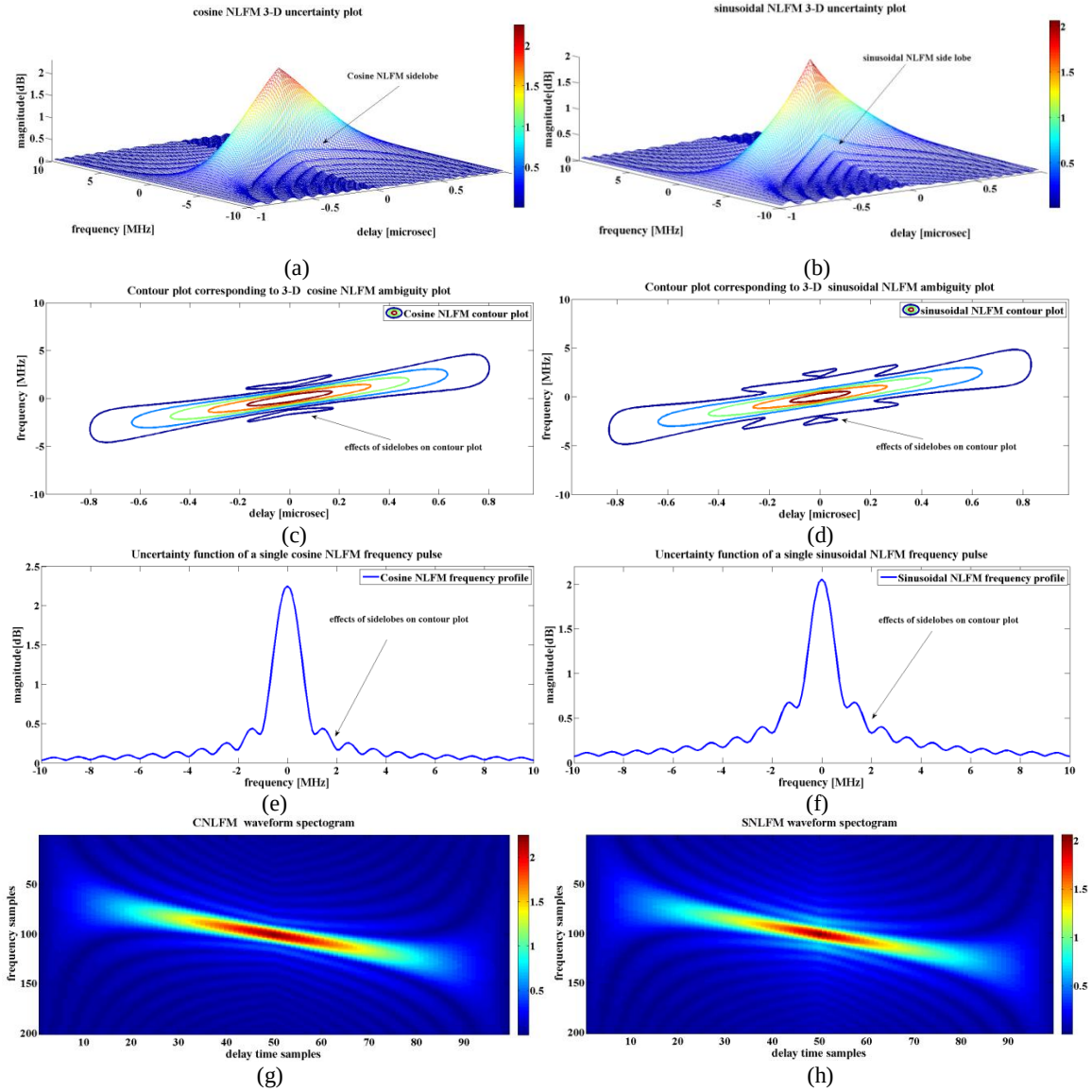

Figure.6. Typical NLFM wave forms AF simulation results (a) CNLFM ambiguity diagram (b) SNLFM ambiguity diagram (c) CNLFM ambiguity contour levels (d) SNLFM ambiguity contour levels (e) CNLFM AF frequency profile (f) SNLFM AF frequency profile (g) CNLFM AF spectrogram (h) SNLFM AF spectrogram

It should be noted that the ideal ambiguity diagram is similar to a single peak of infinitesimal thickness at the center and being zero everywhere else. The single spike implies no ambiguity, and its infinitesimal thickness at the center allows the delay time and Doppler variation to be determined at the same time accurately, but this is impossible to achieve in practice. On the other hand, if the peak is made too narrow, the requirements for a constant volume would cause other smaller peaks to form in areas other than the center, generating ambiguities. In other words, the requirements for ambiguity diagrams and exact resolution accuracy of SAR based on NLFM waveforms generation are not possible to achieve simultaneously. Hence, according to AF qualitative analysis, the continuous CNLFM with its compact contour levels and lesser side-lobes is more proper for implementation and evaluation.

c. CNLFM echo model analysis

According to flight geometry and receive model of SAR in Fig. 1, the SAR received signal strength is always affected by the antenna radiation pattern in the flight direction namely, azimuth time or slow time. This dependency on the azimuth direction emerges in the received incoming continuous CNLFM waveform as Eq. (7):

$$s_r(t_r,t_a) = \mathrm{A}\,.\,w_r\left(t_r-\frac{2R(\mathrm{t}_a)}{c}\right)w_a(\mathrm{t}_a)\ \times\cos\left\{2\pi f_0\left(t_r-\frac{2R(\mathrm{t}_a)}{c}\right)+\pi K_r\left(t_r-\frac{2R(\mathrm{t}_a)}{c}\right)^2+\cos\left(t_r-\frac{2R(\mathrm{t}_a)}{c}\right)\left(t_r-\frac{2R(\mathrm{t}_a)}{c}\right)+\psi\right\} \quad (7)$$

Here, $\mathrm{t_r}$ is the range time, $\mathrm{s_r(t_r,t_a)}$ is the received back scattered signal from the target, A is the received signal amplitude, $\mathrm{w_r(.)}$ is the received pulse envelope, $\mathrm{w_a(.)}$ is the transmitted pulse envelope in azimuth, $\mathrm{f_0}$ is the carrier frequency, $\mathrm{K_r}$ is the chirp rate and c is the speed of the light. The variable of ψ is accounted for phase change in radar signal upon reflection from the surface or induced by platform motions. The presented analysis is unaffected, on the supposition that they are measured and compensate with ancillary sensor unit in the radar motion compensation unit. The received signal in Eq. (7), contains the radar carrier, $cos\{2\pi f_0(t_r-2\,R(t_a)/c)\}$, which is removed before sampling by a quadrature demodulation unit. The final LTI demodulated received baseband CNLFM signal model of a single point scatterer can be represented by the complex form of Eq. (8):

$$s_r(t_r,t_a) = \exp\left\{-j4\pi f_0\frac{R(\mathrm{t}_a)}{c}\right\}\exp\left\{j\pi K_r\left(t_r-\frac{2R(\mathrm{t}_a)}{c}\right)^2\right\}\exp\left\{j\pi\ \cos\left(t_r-\frac{2R(\mathrm{t}_a)}{c}\right).\left(t_r-\frac{2R(\mathrm{t}_a)}{c}\right)\right\} \quad (8)$$

According to Fig. 1, in the case of straight flight path with broadside radiation, the slant range distance between the platform and a point target can be expressed as Eq. (9) [12]:

$$R(\mathrm{t}_a) = \sqrt{(x_i - vt_a)^2 + {r_i}^2}$$

$$R(\mathrm{t}_a) = \sqrt{(R_0\cos\alpha - vt_a)^2 + (R_0\sin\alpha)^2}$$

$$R(\mathrm{t}_a) = \sqrt{{R_0}^2 - 2vR_0\cos\alpha t_a + v^2{\mathrm{t}_a}^2}$$

$$\alpha + \theta = 90 \quad (9)$$

Where, v is the velocity of platform, R0 is slant range at the center of the aperture, α is the squint angle measured between R0 and zero Doppler plane, θ is the equivalent squint angle, and (x_i, r_i) is the point scatterer location over the target terrain. Hence, to investigate the performance of the proposed continuous CNLFM waveform, the SAR simulations are done based on system parameters in Table. 1

Table 1: SAR system parameters

Parameter	**Value**	**Unit**
Modulation type	CNLFM	-
Carrier frequency	15	GHz
Radar transmitter bandwidth	50	MHz
Chirp rate	5×10^{12}	Hz/Sec
Pulse width	10	μsec
Azimuth sampling rate	2	KHz
Range sampling rate	60	KHz
Initial slant range	9452.2	Meter
Minimum slant range	9152	Meter
Maximum slant range	10947	Meter
Platform velocity	800	*m*/sec

The magnitude differences of SAR signal envelope for both of the continuous CNLFM and the continuous SNLFM with the LFM waveform on the basis of Table 1 are shown in Fig.7. The non-linear inherent characteristic of NLFM is the reason of difference in magnitude differences.

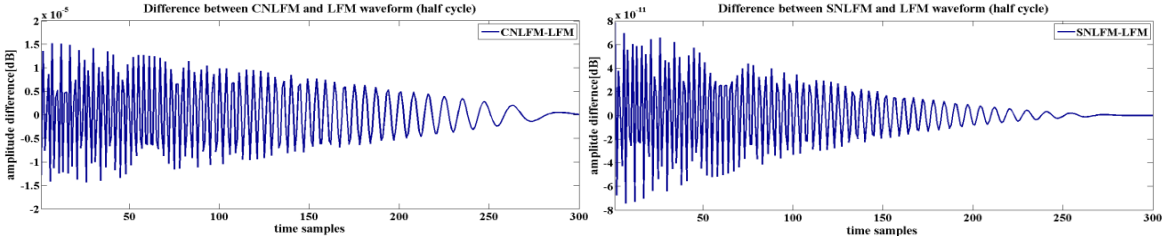

(a) (b)

Figure.7. NLFM envelope difference with LFM (a) CNLFM difference (b) SNLFM difference

III. SAR IMAGE FORMATION ALGORITHM QUALITY ANALYSIS BASED ON NLFM WAVEFORMS

This section simulates the resulted images of received backscattered signal from single point target on the basis of continuous CNLFM, continuous SNLFM and LFM waveforms with the help of RDA [12]. All the simulations are done based on the presumption of similar supersonic flight trajectory with the velocity of 800(m/sec) and the platform motion stability. According to flight geometry in Fig.1 and with the help of Eq. (8), the modified RDA processing procedure is proposed as Fig.8. It should be noted that the effects of flight trajectory is embedded within the received signal model, as well as changes were made to the RDA because of different input waveforms.

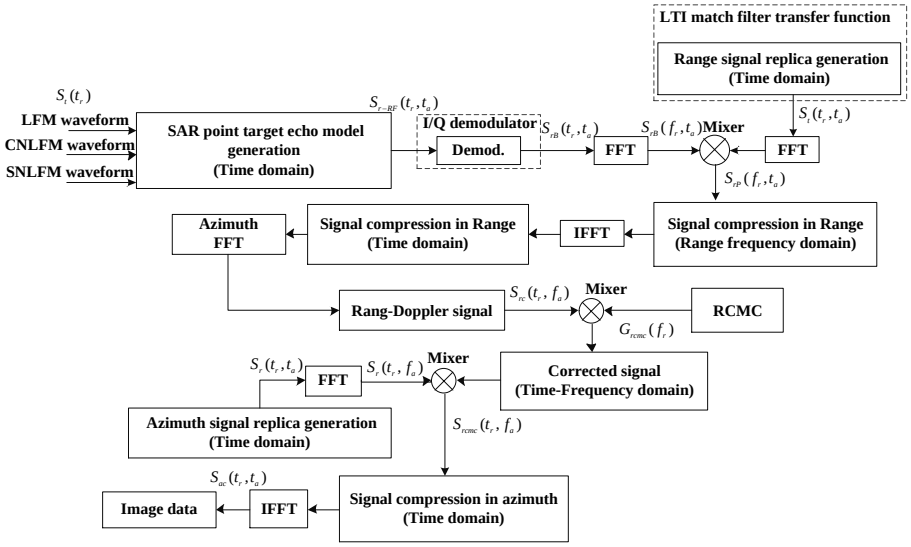

Figure.8. Modified Range-Doppler IFA for the proposed supersonic SAR

a. Raw data generation

The RF input, $s_{r-RF}(t_r, t_a)$, usually passes through one or two stages of analogue down conversion to generate an intermediate frequency (IF) signal, $s_{r\text{-}IF}(t_r, t_a)$, that is directly transformed in to baseband, $s_{rB}(t_r, t_a)$, by I/Q modulator which is generated with the help of Eq. (8) and according to Fig1. Figure 9(a) and 9(b) depict the non-linear characteristic of the non-linear frequency modulation of the generated raw data, $s_{rB}(t_r, t_a)$, of the continuous CNLFM and the SNLFM waveforms. On the other hand, Fig. 9(c) shows that continuous CNLFM waveform is dealing with hyperbola cross junction curves in its generated baseband raw data which is the main impact of CNLFM AF contour levels and is a sign of single point scatterer existence in the middle of the terrain.

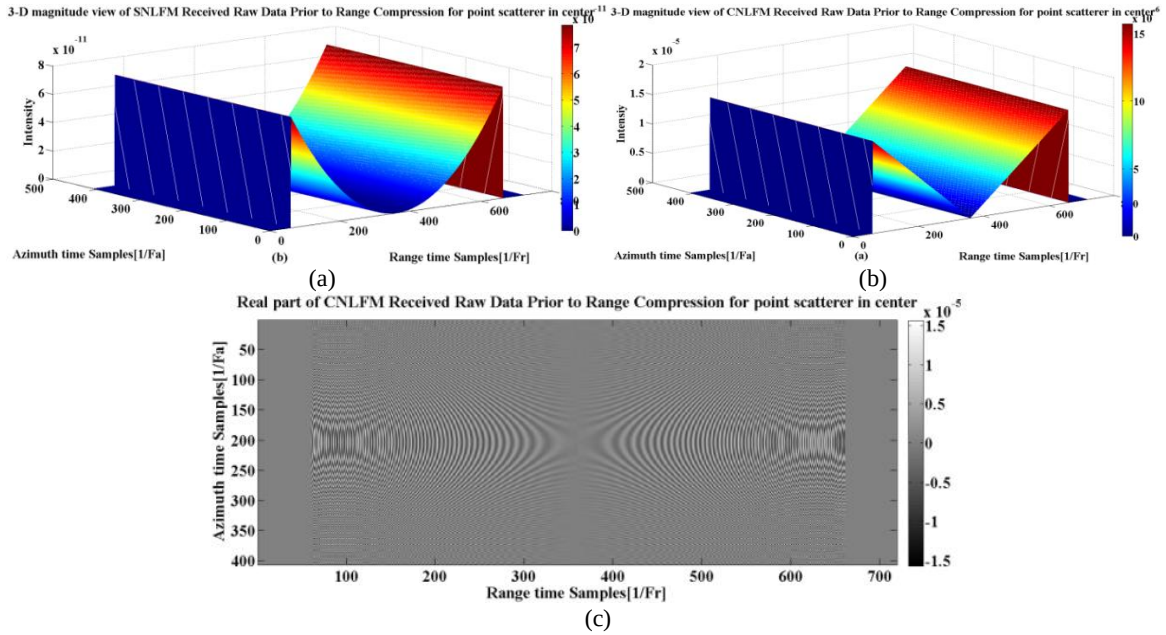

Figure 9. 3D-view of Generated raw data (a) continuous SNLFM waveform (b) continuous CNLFM waveform (c) real part of the single point scatterer in the center of target terrain with continuous CNLFM waveform

b. Range compression

Range compression is done via a fast convolution when the data are in the azimuth time domain. In the other words, a range FFT is performed,(f_r, t_a), on Eq. (8) followed by a range match filter multiply,$H(f_r)$, and finally a range IFTT completes the range compression as Eq.(10):

$$s_{rc}(t_r, t_a) = IFFT_r\{s_r(f_r, t_a).H(f_r)\} = A.P_r\left[t_r - \frac{2R(t_a)}{c}\right] W_a(t_a - t_c)\exp\left\{-j4\pi f_0 \frac{R(t_a)}{c}\right\} \quad (10)$$

Where, $s_r(t_r, t_a)$ is the generated raw data, $P_r(t_r)$ is the IFFT of the window $w_r(f_r)$, $s_r(f_r, t_a)$ is the range FFT of $s_r(t_r, t_a)$, $H(f_r)$ is the match filter function and $s_{rc}(t_r, t_a)$ is the range compressed spectral equation. The value of A is supposed to unit in order to compare the result of LFM, continuous CNLFM and continuous SNLFM implementation in the final image. For a rectangular window or tapered window, $P_r(t_r)$ is a sinc function or a sinc-like function with lower side-lobes.

c. Azimuth FFT transform

An azimuth FFT transforms the data into the Range-Doppler domain (t_r, f_a) as Eq. (11):

$$S_1(t_r, f_a) = FFT_a\{s_{rc}(t_r, t_a)\} = A.P_r\left[t_r - \frac{2R(f_a)}{c}\right] W_a(f_a - f_c)\exp\left\{-j4\pi f_0 \frac{R_0}{c}\right\}\exp\left\{j\pi \frac{{f_a}^2}{K_a}\right\} \quad (11)$$

Where, $S_1(t_r, f_a)$ is an azimuth FFT transform of range compressed data in the Doppler domain. The azimuth beam pattern $w_a(t_a - t_c)$ is transformed into, $W_a(f_a - f_c)$, with its shape preserved. The second phase term is the azimuth modulation which also has LFM and NLFM characteristic

in, f_a, while the first exponential term carries the inherent phase information of the target. The value of f_c is due to center frequency and center time, t_c.

d. Range Cell Migration Correction (RCMC)

RCMC is the range time and frequency dependent, is performed in the Range-Doppler domain, (t_r, f_a). The amount of RCM to correct is given by (ΔR_{f_a}) which is a function of azimuth frequency and represents the target displacement. Note that $\Delta R_{f_a}$is also a function of R_0 that is the range variant. The total procedure of RCMC is:

$$\Delta R_{f_a} = \frac{\lambda^2 R_0 {f_a}^2}{8 {v_r}^2}$$

$$G_{rcmc}(f_r) = \exp\left\{j\frac{4\pi f_r \Delta R_{f_a}}{c}\right\}$$

$$S_{rcmc}(t_r, f_a) = S_2(t_r, f_a).G_{rcmc}(f_a)$$

$$S_2(t_r, t_a) = IFFT_a\{S_{RCMC}(t_r, f_a)\} \quad (12)$$

Where, $\Delta \mathrm{R_{f_a}}$ is the amount of RCM which has LFM and NLFM characteristic in, f_a, $\mathrm{G_{rcmc}(f_r)}$ is the phase term of RCM, $\mathrm{S_{RCMC}(t_r, f_a)}$ is the corrected signal with RCMC and $\mathrm{S_2(t_r, t_a)}$ is the corrected signal in both range time and azimuth time.

e. Azimuth match filtering

Since the data after RCMC are in the Range-Doppler domain, (t_r, f_a), it is convenient and efficient to implement the azimuth match filter in this domain as a function of slant range, R_0, and azimuth frequency, f_a. This step can be performed as the frequency domain match filter, $H_a(f_a)$, multiply at each range gate as Eq.(13):

$$\mathrm{K_a} \approx \frac{2{\mathrm{v_r}}^2}{\lambda \mathrm{R_0}}$$

$$\mathrm{H_a(f_a)} = \exp\left\{-\mathrm{j}\pi\frac{{\mathrm{f_a}}^2}{\mathrm{K_a}}\right\}$$

$$\mathrm{S_3(t_r, f_a)} = \mathrm{S_2(t_r, f_a).H_a(f_a)} = A.P_r\left[t_r - \frac{2R_0}{c}\right]W_a(f_a - f_c)\exp\left\{-j4\pi f_0 \frac{R_0}{c}\right\} \quad (13)$$

Where, $\mathrm{H_a(f_a)}$ is the frequency domain match filter, $\mathrm{K_a}$ is the function of $\mathrm{R_0}$ and $\mathrm{S_3(t_r, f_a)}$ is the azimuth compression after RCMC.

f. Azimuth IFFT

This step, transforms the data back to the time domain and results in the complex data as Eq.(14):

$$\mathrm{S_{ac}} = \mathrm{IFFT\{S_3(t_r, f_a)\}} = A.P_r\left[t_r - \frac{2R_0}{c}\right]P_a(t_a)\exp\left\{-j4\pi f_0 \frac{R_0}{c}\right\}\exp\{j2\pi f_c t_a\} \quad (14)$$

Where, $P_a(.)$ is the amplitude of the azimuth impulse response, a sinc function similar to, P_r. The first exponential shows the target phase due to its range position, R_0, and the second is the phase term due to Doppler center frequency which has LFM and NLFM frequency modulation

characteristics. Accordingly, the final results of RDA using LFM, continuous SNLFM and the continuous CNLFM waveforms are shown in Fig.10 and Fig.11.

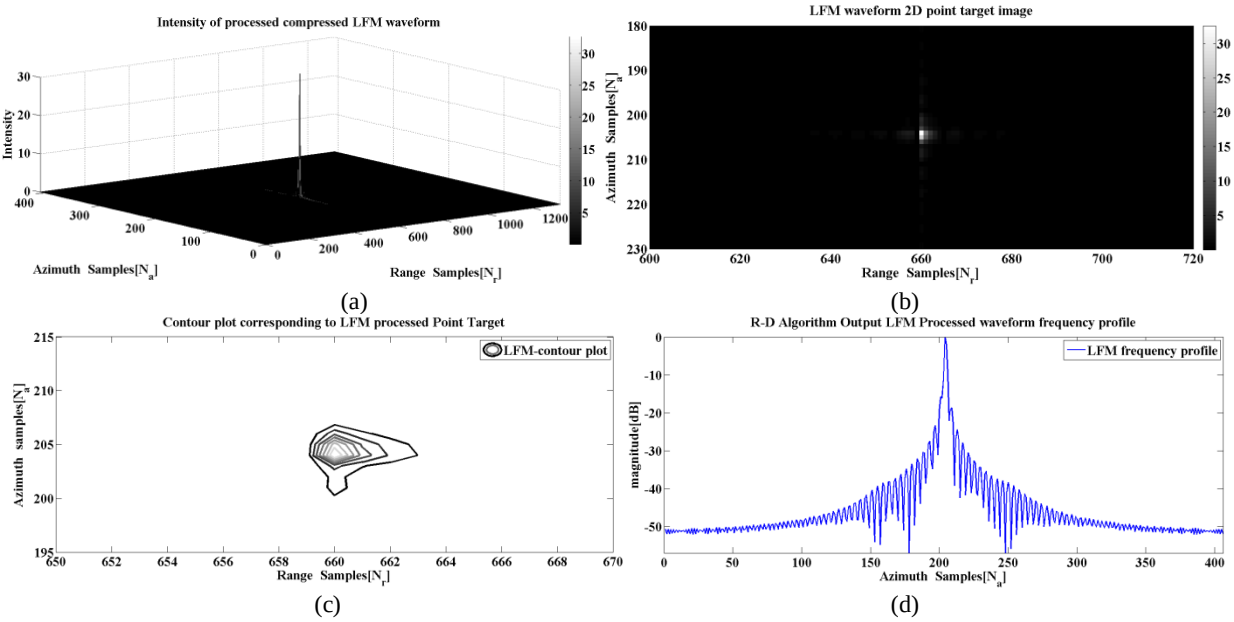

Figure 10. Final RDA image of single point scattrer with LFM waveform (a) 3D-view after azimuth compression (b) 2D-view of target spectral expansion (c) 2D-view of scatterer contour levels (d) received frequency profile of target

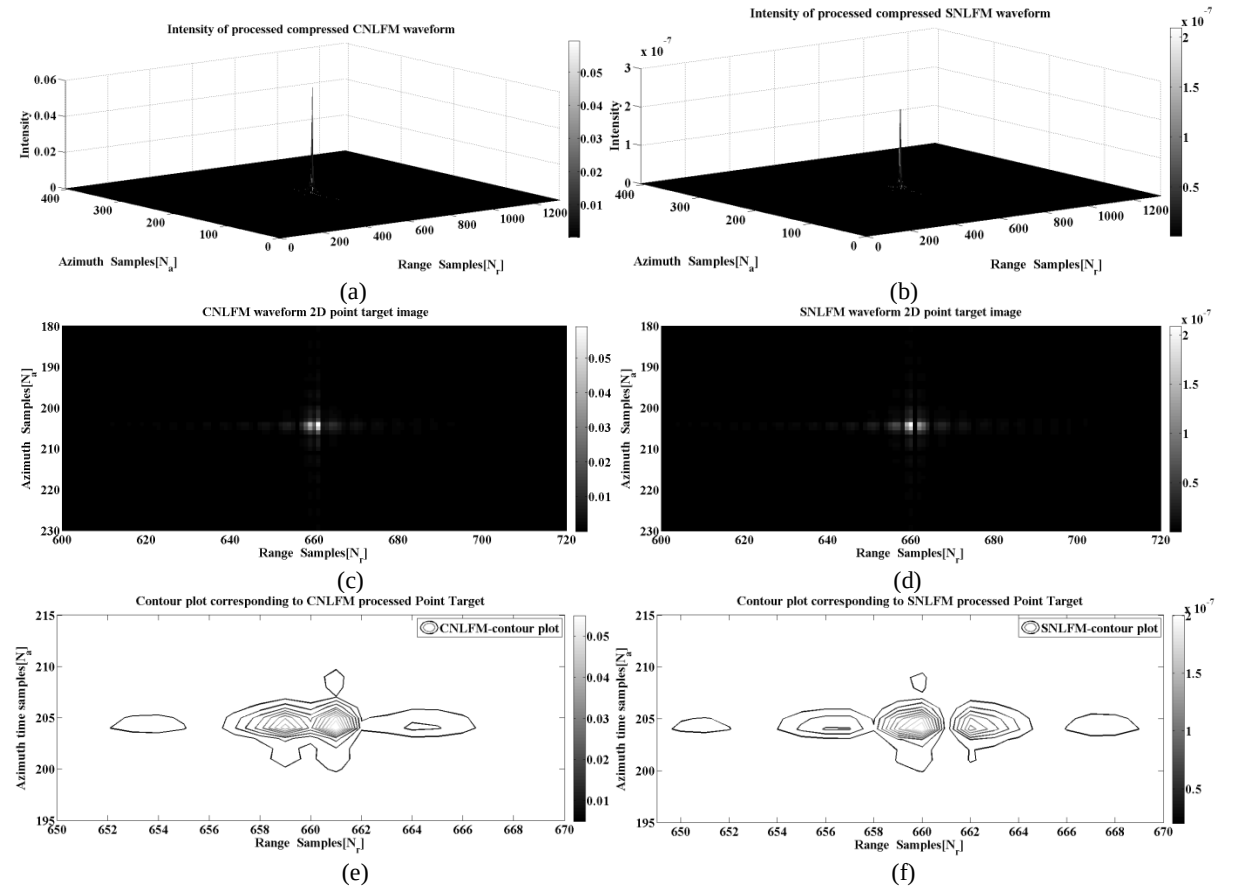

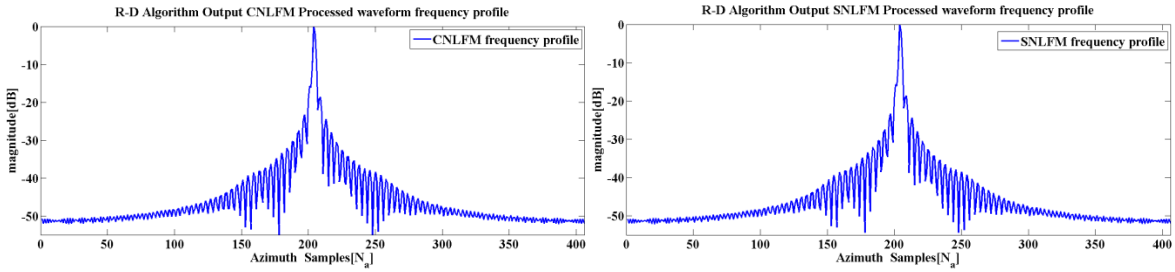

(g) (h)

Figure 11. Final RDA image of single point scattrer with CNLFM and SNLFM waveform (a) CNLFM 3D-view after azimuth compression (b) SNLFM 3D-view after azimuth compression (c) CNLFM 2D-view of target spectral expansion (d) SNLFM 2D-view of target spectral expansion (e) CNLFM 2D-view of scatterer contour levels (f) SNLFM 2D-view of scatterer contour levels (g) CNLFM received processed frequency profile of target (h) SNLFM received processed frequency profile of target

According to spectral expansion simulation results in Fig. 10(b), 11(c) and 11(d) it is evident that waveform plays a key role in the pixel overlapping on the basis of non-linearity behavior of quadratic phase modulation which directly affects the spectrum weighting and the reconstructed images . Similarly, the phase contour levels as shown in Fig. 10(c), 11(e) and 11(f) also have the same results while being analyzed on the basis of inherent non-linear modulation characteristics and with the help of phase modulation that provides very smaller side-lobe levels. The difference between Fig. 10(c), 11(e) and 11(f) is the result of existing differences of the AF contour levels in Fig. 5(b), 6(c) and 6(d). Likewise, frequency profiles are derived as Fig. 10(d), 11(g) and 11(h). In Fig.12, It is obvious that Fig. 10(d), 11(g) and 11(h) are different as a result of the AF frequency profiles which are mentioned in Fig. 5(c), 6(e) and 6(f). Hence, the total procedure of the AF quality analysis of continuous NLFM waveforms verifies that CNLFM waveform has more effects on the image contrast in comparison to SNLFM and as an alternative to LFM. On the other hand, to find the differences between SNLFM and CNLFM, quantitative quality metrics would be a key which are to be done on the reconstructed images in next section.

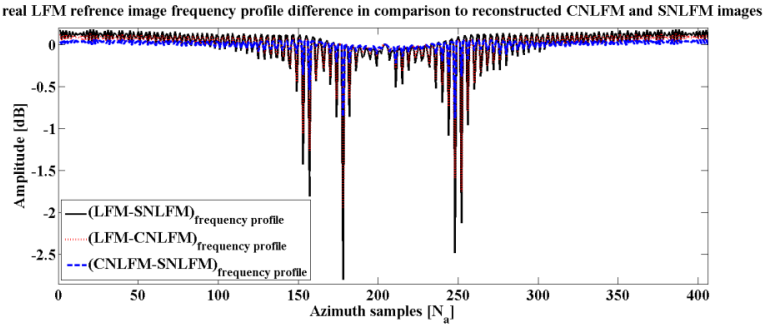

Figure 12. Frequency profile difference presentation of LFM, SNLFM and CNLFM

IV. SAR IMAGE FORMATION OBJECTIVE QUALITY ASSESSMENT EVALUATION

This section introduces and implements full-reference objective image quality assessment metrics on reference resulted LFM image and reconstructed NLFM images which are shown in Fig. 10(a), 11(a), and 11(b) under both the noise-free and noisy target terrain situations.

a. Objective NLFM waveforms image quality assessment metric definitions

The full-reference objective image quality metrics includes the mean value, variance, SNR, PSNR, MSE, PSD, NCC and the ISLR. The Mean and Variance values of the SAR images are statistical behavior information presentation which helps to analyze the probability of maximum likelihood of the reconstructed images. Mean value gives the contribution of individual pixel intensity for the entire SAR image and variance is normally used to find how each pixel varies from the neighboring pixel or center pixel within an image. The SNR is calculated as the ratio of the mean value of the image and the standard deviation of the noise within the image. The higher the SNR value, the sharper the reconstructed NLFM images will be. The PSNR is the ratio between the maximum possible power of the image and the power of corrupting noise that affects the quality of the image with the help of MSE as a scaled definition of power by the number of pixels in the images. There is an inverse relationship between PSNR and MSE. So, the higher the PSNR value indicates the higher quality of the reconstructed NLFM images which introduces the lower value of errors.

The PSD as a major quality assessment metric is also measures the strength of the energy as a function of frequency which shows at which frequencies variations are strong and at which frequencies variations are weak. The PSD is the best way to study the Non-linear modulation characteristics of the implemented NLFM waveforms in the SAR applications. The NCC is used as a criterion to evaluate the degree of similarity between the LFM image as the reference waveform and the reconstructed CNLFM and SNLFM images which are proposed to replace the LFM.

In addition to the qualitative comparison analysis based on the AF diagrams and aforementioned objective image quality metrics, ISLR is another important metric in SAR image quality assessment techniques. The ISLR measurement is done in a square area with 10 cells width and a center of maximum amplitude.

In this paper it is basically focused on the NLFM waveforms generation and their effects on the quality of the reconstructed images while the SAR is dealing with noise-free and noisy target terrain situations. It should be noted that the noisy conditions do not affect the entity of the objective image quality metrics assessment but the result values would be different in comparison to noise-free situation. Hence, both the noisy and noise-free target terrain situations could be called as NLFM waveform quality assessment in CRM.

b.Objective NLFM waveforms quality assessment simulation in the CRM

According to Section IV.A while the SAR is dealing with the noise-free conditions, the pixel difference-based measurements results are derived as Table 2. It shows that the input reference LFM image has an SNR of 52.14dB. The value of about 0.8dB difference in the SNR value of CNLFM and SNLFM confirms that CNLFM affects the image quality better than SNLFM. It should be noted that a noise-free target terrain usually has SNR values higher than 50dB and the simulations verify the process of objective image quality metrics assessment. The mean and variance values are used in cases when it is totally deduced that the images to be analyzed are exactly the same visually. These values related to the both of the SNLFM and CNLFM in comparison to LFM are listed in Table 2, which are the results of Fig.6 (e) and 6(f). The importance of these differences will be emerged while dealing with the noisy target terrain situation quality metrics assessment.

Table 2: Pixel based measurement values in the noise-free target terrain

Waveform	SNR	Variance	Mean
LFM	52.14 dB	0.005	2×10^{-3}
CNLFM	51.27 dB	4×10^{-13}	2.9×10^{-8}
SNLFM	50.40 dB	6×10^{-24}	1.3×10^{-13}

Accordingly, the PSNR and the MSE values are derived and listed in Table 3.The PSNR calculation also illustrates that both the CNLFM and SNLFM waveforms have the same value because there are testing in noise-free situation and 23dB is acceptable while the MSE value is close to zero.

Table 3: PSNR and MSE values in the noise-free target terrain

Wave form	PSNR	MSE
CNLFM	23.008 dB	0.01
SNLFM	23.008 dB	0.01

In the case of dealing with the similar PSNR value for objective quality metric assessment, SSIM is a suitable alternative to demonstrate the performance of non-linear waveforms implementation in comparison to LFM. According to the presence of the single point scatterer while dealing with the CNLFM and SNLFM waveforms in the noise-free condition, the SSIM difference of CNLFM and SNLFM reconstructed images are presented as Fig.13. So, it is deduced that the CNLFM image reconstruction is a suitable alternative to LFM in comparison to the SNLFM.

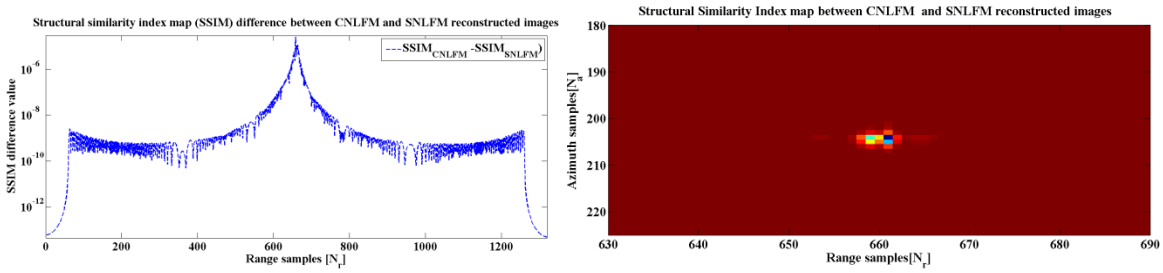

(a) (b)

Figure 13. SSIM amplitude difference between CNLFM and SNLFM in the noise-free target terrain (a) logarithmic magnitude difference (b) 2D-view

Following the objective quality metrics assessment, by applying 2D discrete Fourier transform on the reconstructed CNLFM and SNLFM images, their PSD are calculated. Results in the Fig.14, verifies that CNLFM has better PSD which means that energy distribution as a function of non-linear frequency modulation are stronger in comparison to SNLFM waveforms in the same conditions. On the other hand, the NCC simulation results of CNLFM, SNLFM, an NCC difference about 0.4dB verifies that CNLFM has better effects in the image reconstruction based on cosine modulation in the noise-free target terrain. The results are also shown in Fig. 15.

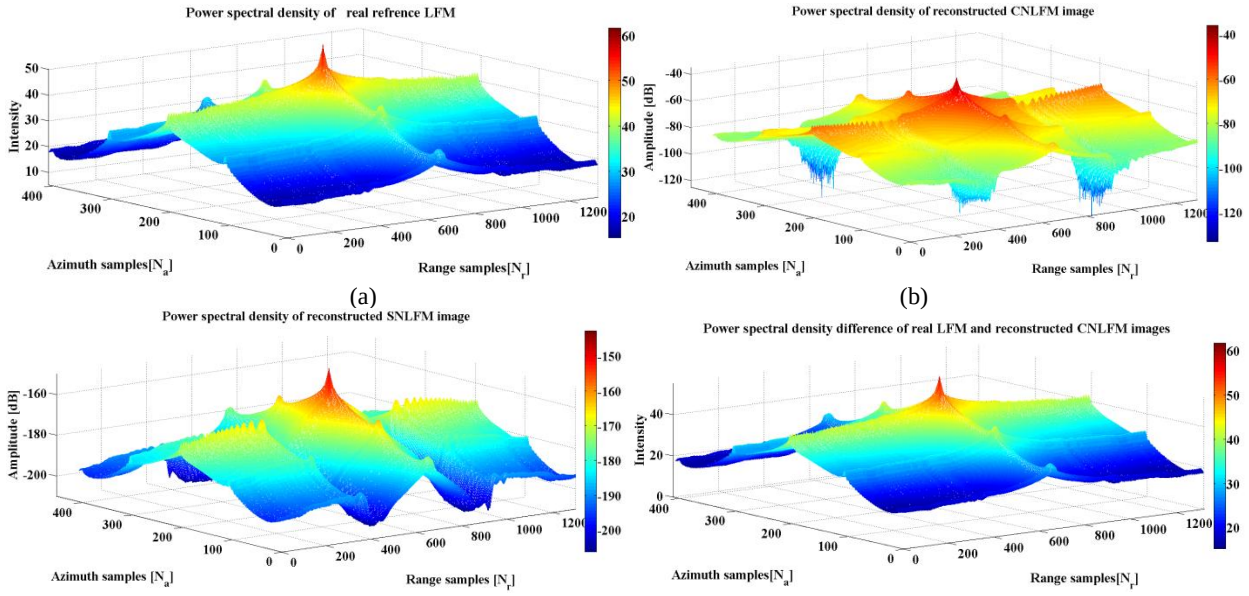

(a) (b)

(c) (d)

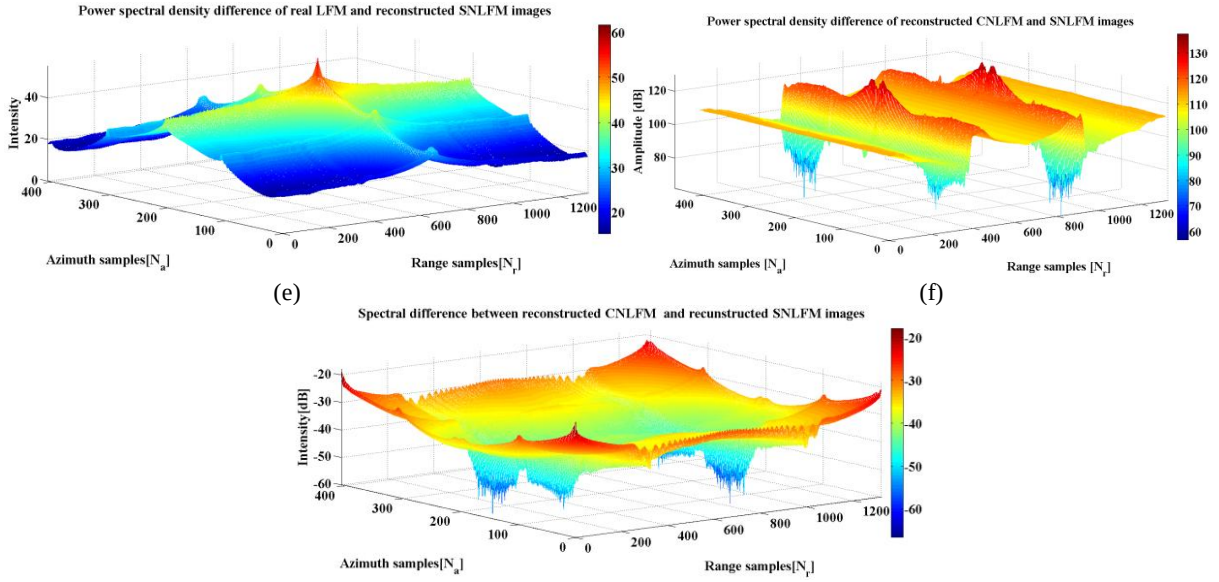

Figure 14. PSD presentation in the noise-free target terrain (a) PSD of real reference LFM (b) PSD of reconstructed CNLFM (c) PSD of reconstructed SNLFM (d) PSD difference between LFM and reconstructed CNLFM (e) PSD difference between LFM and reconstructed SNLFM (f) PSD difference between reconstructed CNLFM and SNLFM (g) spectral difference between reconstructed CNLFM and SNLFM images

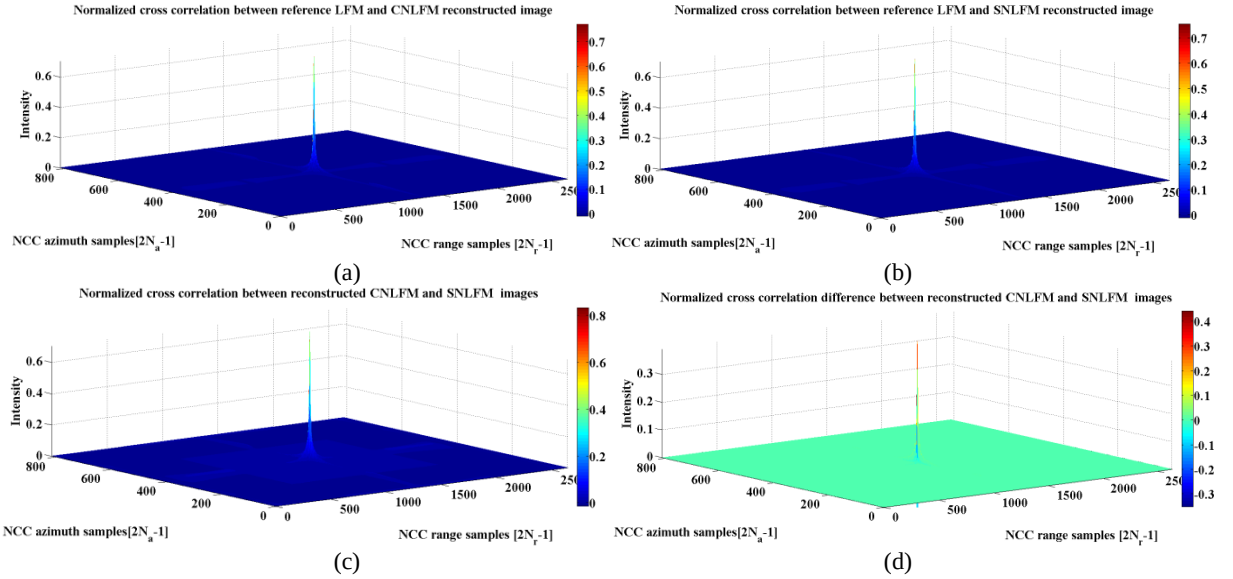

Figure 15. NCC presentation in the noise-free target terrain (a) NCC of reconstructed CNLFM and LFM (b) NCC of reconstructed SNLFM and LFM (C) NCC of reconstructed CNLFM and SNLFM (d) NCC difference between reconstructed CNLFM and SNLFM images

Then, to investigate the robustness of the proposed CNLFM waveform in the noisy target terrain situation, additive white Gaussian noise (AWGN) with constant mean and variance values based on Table 2, is added to the image intensity for further quality metric assessments. The process of adding the AWGN to the images is done by two methods. Firstly, the AWGN is applied directly

to the reconstructed images based on their own variance and mean values. Secondly, for the purpose of the NLFM robustness analysis, the variance and mean values of the real LFM reference image will be considered as the criterion for adding AWGN to the other CNLFM and SNLFM reconstructed images. Then, objective image quality metrics assessment will be done. Figure 16 presents the image of point scatterer in the noisy condition based on their own values.

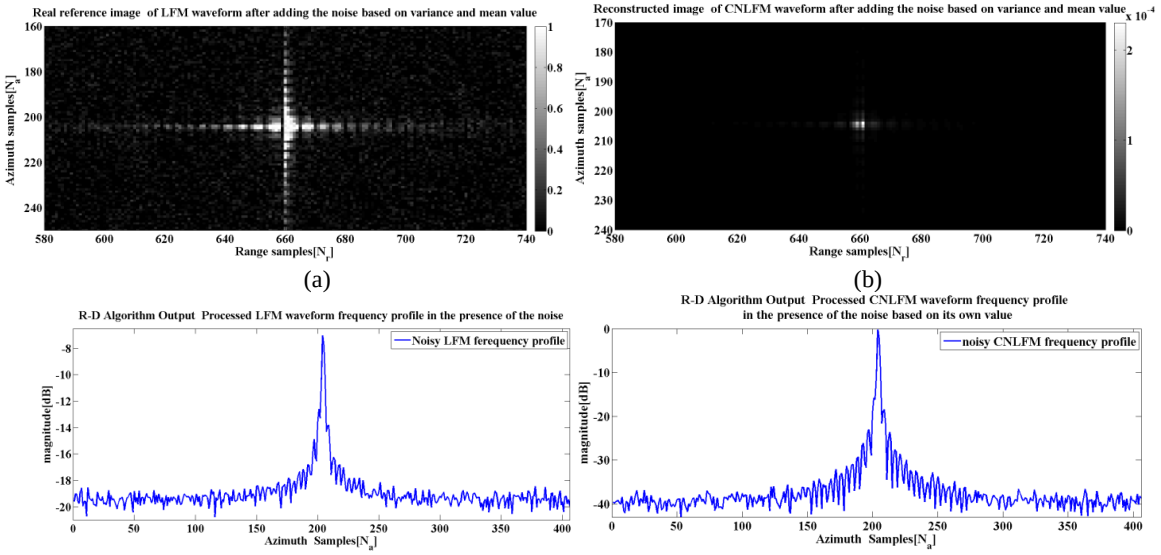

Figure 16. Image presentation in the noisy target terrain based on their own variance and mean values (a) LFM real reference image (b) CNLFM reconstructed noisy image (c) LFM real reference image frequency profile(d) CNLFM reconstructed noisy image frequency profile

It should be noted that the SNLFM reconstructed noisy image is the same as Fig. 16(b) visually. The objective image quality metrics assessments based on pixel-difference based method are listed in Table 4. The PSNR and MSE values in the noisy target terrain are also derived and listed in Table 5.The PSNR calculation also illustrates that both the CNLFM and SNLFM waveforms have the same value while the MSE value is zero because of the AWGN presence.

Table 4: Pixel based measurement values in the noisy target terrain based on their own value

Wave form	SNR	Variance	Mean
LFM	26.91dB	2×10^{-3}	0.0304
CNLFM	46.87 dB	5.53×10^{-13}	2.8×10^{-7}
SNLFM	45.98 dB	8.34×10^{-24}	1.17×10^{-12}

Table 5: PSNR and MSE values in the noisy target terrain based on their own value

Wave form	PSNR	MSE
CNLFM	25.2 dB	0.00
SNLFM	25.2dB	0.00

The NCC simulations under noisy target terrain situation based on the first method are shown in Fig. 17. The NCC simulation verifies that adding AWGN will affect the image reconstruction but the effects are not enough for target dissolving within the images. So, proposed CNLFM are robust to the noise. The same result of robustness is also deduced for the SNLFM waveform which is shown in the SSIM form in Fig. 17(d).

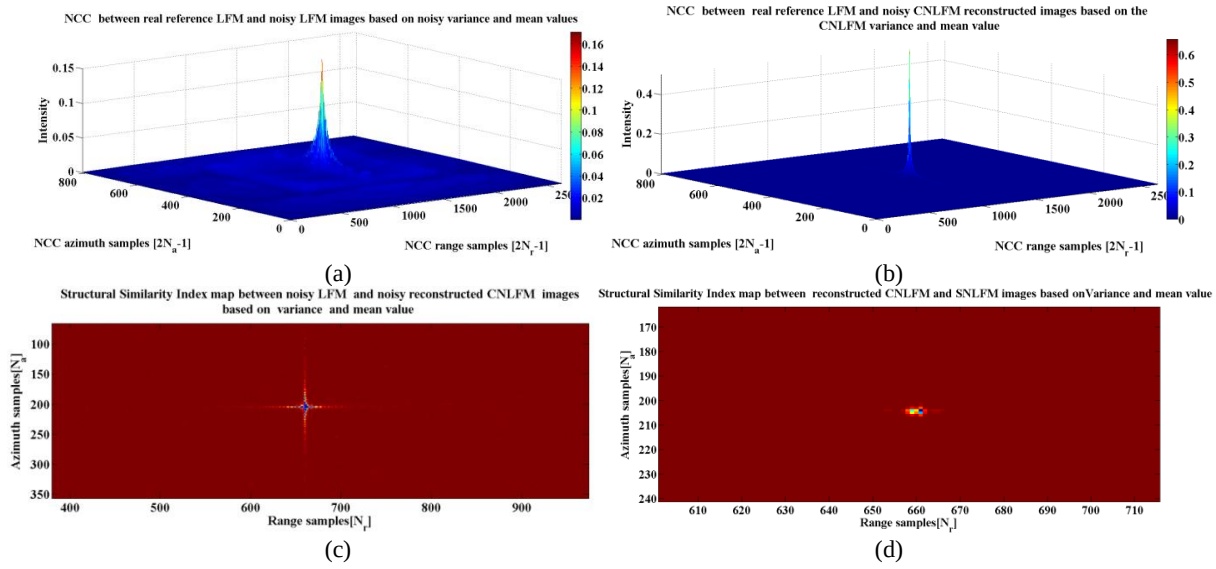

Figure 17. NCC presentation in the noisy target terrain based on their own variance and mean values (a) NCC of real reference LFM and noisy LFM (b) NCC of reconstructed noisy CNLFM and real reference LFM (c) SSIM between LFM and reconstructed CNLFM (d) SSIM between reconstructed CNLFM and SNLFM

Now, considering next method of noisy target terrain based on the variance and mean values of the real reference LFM as AWGN criterion which are applied directly to both the reconstructed CNLFM and SNLFM images. In comparison to Fig. 16(b) the reconstructed noisy SNLFM and CNLFM images are quite disrupted and the point scatterer is dissolved within the images as shown in Fig. 18. The frequency responses in Fig. 18(c) and 18(d) are quite different from 16(c) and 16(d) which results from the implementation of AWGN based on real reference LFM image.

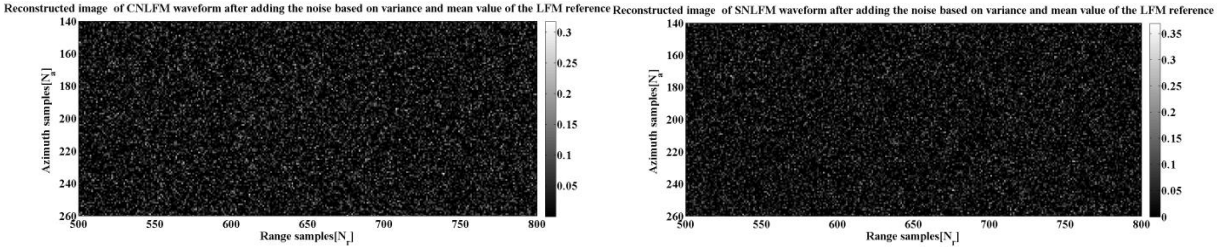

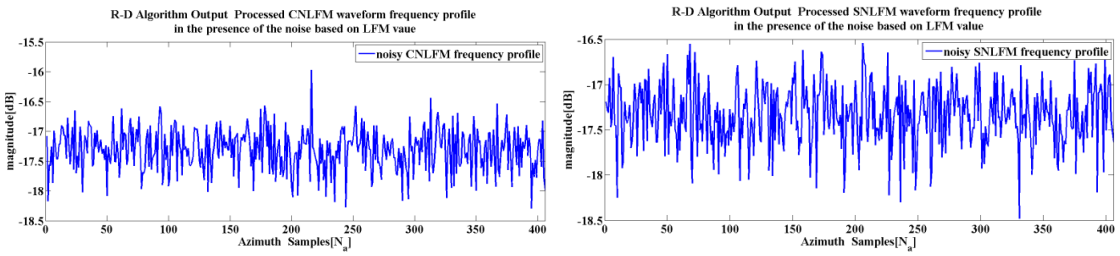

(c) (d)

Figure 18. Image presentation in the noisy target terrain based on LFM variance and mean values (a) CNLFM reconstructed noisy image (b) SNLFM reconstructed noisy image (c) CNLFM reconstructed noisy image frequency profile frequency profile(d) SNLFM reconstructed noisy image frequency profile

Furthermore, the objective quality metrics assessment based on pixel-difference based method for the noisy target terrain on the basis of LFM values are listed in Table 6 and Table 7.

Table 6: Pixel based measurement values in the noisy target terrain based on LFM values

Wave form	SNR	Variance	Mean
LFM	26.89 dB	0.002	0.0304
CNLFM	18.79 dB	0.0018	0.293
SNLFM	17.71 dB	0.0018	0.291

Table 7: PSNR and MSE values in the noisy target terrain based on LFM values

Wave form	PSNR	MSE
CNLFM	24.18 dB	0.00
SNLFM	24.19 dB	0.00

The NCC simulations under noisy target terrain situation based on the second method are shown in Fig. 19. The results in Fig.19 (a) and 19(b) verify that adding AWGN based on the LFM variance and mean values affect the image reconstruction to the extent of the target dissolving within the medium. So, the proposed CNLFM and SNLFM waveform are suitable alternatives for LFM while dealing with noisy condition based on their own parameters. The SSIM between reconstructed SNFLM and CNLFM under second noisy condition verifies the importance of the non-linear frequency modulation in SAR while dealing with CRM.

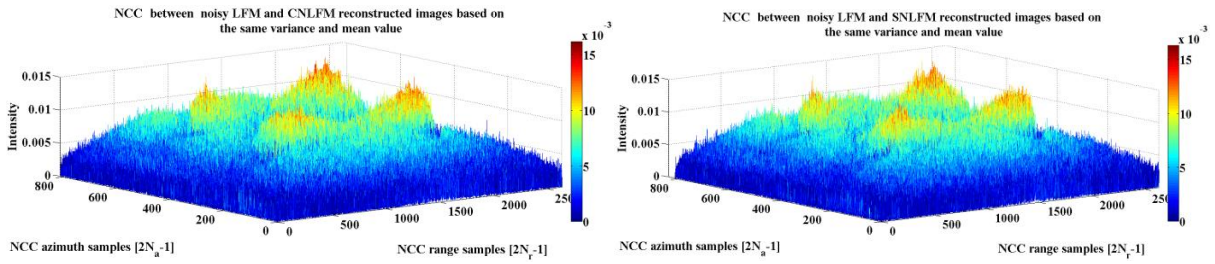

(a) (b)

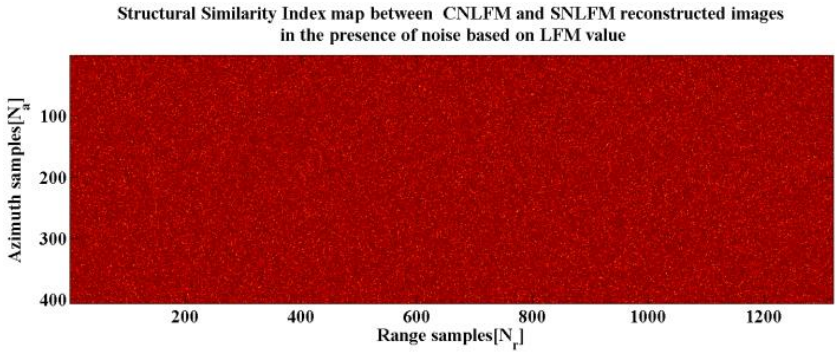

(c)

Figure 19. Image presentation in the presence of the noise based on LFM parameters (a) real reference LFM image (b) reconstructed CNLFM image (c) SSIM between reconstructed CNLFM and SNLFM

According to, Table. 1 and results in Fig. 10(b), 11(a), 11(b), 16(a), 16(b), 18(a) and 18(b) the ISLR value for the LFM, continuous SNLFM and the continuous CNLFM in the CRM target terrain are calculated and listed as Table. 8. For the sake of precise ISLR measurement both of the range and the azimuth directions were taken into accounts. It is evident that the ISLR value as an objective quality metric criterion which is used specifically in SAR image quality assessment techniques, verifies that CNLFM has better performance in comparison to other non-linear waveform. The result simulations based on ISLR not only confirms that NLFM waveform is a suitable alternative for LFM but also is a proper method while dealing with CRM target terrain. According to Table 8, it is also evident that CNLFM has better quality effects on the image in comparison to SNLFM.

Table 8: Objective quality ISLR value in the CRM target terrain

ISLR value	**Original waveform**			**Noisy waveforms**				
				Based on their own Variance and Mean value			**Based on LFM Variance and Mean value**	
	LFM	SNLFM	CNLFM	LFM	SNLFM	CNLFM	SNLFM	CNLFM
Range[dB]	-12.91	-12.50	-12.86	11.05	-12.7	-14.84	9.4	8.89
Azimuth[dB]	-12.92	-7.23	-9.63	15.85	-4.06	-7.3	16.7	19.93

V. CONCLUSION

This article compares the characteristics of LFM, continuous SNLFM and continuous CNLFM waveforms based on their AF quality analysis and subsequently, the optimum continuous CNLFM waveform is proposed for further analysis. The impact of CNLFM implementation was investigated in comparison to LFM and SNLFM with the help of objective image quality

assessment metrics analysis in the CRM target terrain situations. All the simulations were carried out based on similar flight trajectory and system parameters while complete objective image quality assessment metrics were designated to the each of simulation results and compared to each other. The variance value, mean value, SNR, PSNR, SSIM, MSE, PSD, NCC and ISLR value in both the range and azimuth directions were extracted and compare based on their waveforms and medium which is considered as CRM. All the results validate that CNLFM waveform is not only a suitable alternative for LFM but also is more robust to SNLFM and even in some cases to LFM. As verified by the metrics and simulation results, the PSD of CNLFM in comparison to SNLFM and LFM is more efficient for using in noisy conditions, which means the robustness of the waveform in CRM. In the following, the ISLR comparison results show that the continuous CNLFM waveform not only reduces the level of the side-lobes but also increase the main lobe and makes the image formation algorithm more robust in face of dealing with spectral expansion and Doppler deviations in the image while dealing with CRM target terrain. The -13dB and -15dB, ISLR value is quite acceptable in SAR image formation. The total quality assessment solution for the proposed waveform generation method in SAR while dealing with CRM are carried out based on the qualitative and quantitative analysis which is a complete image quality assessment technique. Future activities in the context of this article might involve using new other waveforms generation and implementation, increasing the squint angle and modifying the image formation algorithm, using the method of time-frequency processing in processing while analyze the Doppler toleration analysis, and also target detection and classification in multiple target terrain.

REFERENCES

[1] J. J. Kovaly., *Synthetic Aperture Radar*., Artech House, Dedham, MA, 1976.

[2] J. C. Curlander, R. N. McDonough, Synthetic Aperture Radar: Systems & Signal Processing, John Wiley & Sons editions, New York.1991.

[3] M. I. Skolnik., *Introduction to Radar Systems*., McGraw-Hill, New York, 2001.

[4] M. Sack, M. R. Ito and I. G. Cumming, "Application of efficient linear FM matched filtering algorithms to synthetic aperture radar processing" IEE Proceedings, Vol. 132, pp. 45-57, Feb. 1985.

[5] R. Sullivan, *Synthetic aperture radar*, in M. I. Skolnik Radar Handbook, 3rd Ed, New York: McGraw Hill, 2008.

[6] J. Zhu, Zh. He, Bo. Zhou and J. Li, "Real-time signal processing implementation of the missile-borne SAR using high performance DSP", IEEE, Int. Conf. on Radar, pp. 1-4, Oct. 2006.

[7] Y. Liu, M. Xing, G. Sun, X. Lv, Z. Bao and W. Hong, "Echo model analysis and imaging algorithm for high-resolution SAR on high-speed platform", IEEE, Trans on Geo. and Rem. Sens., Vol.50, No.3, pp. 933-950,Sept. 2012.

[8] Y.Yusheng, Zh. Linrang, L. Yan, L. Nan and L. Xin, "Range Doppler algorithm for bistatic missile-borne forward-looking SAR", IEEE 2nd APSAR, pp. 960-963, Oct. 2009.

[9] Zh.Yingxi, L. Ming, "A design of motion compensation for high resolution imaging of missile-borne SAR", IEEE, ICCCAS, pp. 427-430, Sept. 2009.

[10] G. Brooker, M. Bishop and R. Hennessy, "Evolution of a suite of smart millimetre wave radar systems for situational awareness and automation in mines", International Journal on Smart Sensing and Intelligent Systems (S2IS), Vol. 1, No. 8, pp.315-353, Jun. 2008.

[11] E. De Witte and H. D. Griffiths, "Improved ultra-low range sidelobe pulse compression waveform design", IEEE Electronics Letters, vol. 40, no. 22, pp. 1448–1450, Nov. 2004.

[12] S. F. Li, J. Chen, L.Q. Zhang and Y.Q. Zhou, "Image Formation Algorithm for Missile-Borne MMW SAR with Phase Coded Waveform", IET, Int. Conf. on Radar, pp. 1-4, Dec. 2009.

[13] James M. Kurdzo, Boon Leng Cheong, Robert D. Palmer, Guifu Zhang, "Optimized NLFM pulse compression waveforms for high-sensitivity radar observations", Int. Radar Conference (Radar), pp.1-6 ,Oct. 2014.

[14] J.Saeedi , Karim Faez, "Synthetic aperture radar imaging using nonlinear frequency modulation signal", IEEE Transactions on Aerospace and Electronic Systems ,Vol. 52, Issue. 1, pp. 99-110, Feb. 2016.

[15] S. Boukeffa, Y. Jiang, T. Jiang, "Sidelobe reduction with nonlinear frequency modulated waveforms", IEEE 7th Int. Colloquium on Signal Processing and its Applications (CSPA), pp. 399-403, May. 2011

[16] M. Luszczyk, "Numerical evaluation of ambiguity function for stepped non-linear FM radar waveform", International Conference on Microwaves, Radar & Wireless Communications (MIKON), pp.1164 – 1167, May. 2006.

[17] Wei Wang, Robert Wang, Yunkai Deng, Zhimin Zhang, Xiayi Wu, Zhihuo Xu, "Demonstration of NLFM Waveforms With Experiments and Doppler Shift Compensation for SAR Application", IEEE Geoscience and Remote Sensing Letters, Vol. 13, Issue 12, pp.1999-2003 , Dec. 2016.

[18] B. R. Mahafza., *MATLAB Simulations for radar System Design*, Chapman & Hall, 2004.

[19] X. Lu and H. Sun, "Parameter assessment for SAR image quality evaluation system " in Proc. 1st APSAR, pp. 58–60, Nov. 2007.

[20] I. Heidarpour, M. Kazerooni, M. Fallah, "A complex target terrain SAR raw data generation and evaluation based on inversed equalized hybrid-domain algorithm processing," Waves in Random and Complex Media (WRCM), Vol. 27, Issue 1, pp.47-66, Jan. 2017.
[21]Y. Fei, Y. Zh. Shan, L. C. Ren and Ch. En, "Image quality assessment method for underwater acoustic communication based on digital watermarking," International Journal on Smart Sensing and Intelligent Systems (S2IS), Vol. 6, No. 2, pp.752-771, Apr. 2013.
[22] F. J. Harris, "On the Use of Windows for Harmonic Analysis with the Discrete Fourier Transform", Proceedings of the IEEE. Vol. 66, pp. 51-84, Jan. 1978.